A Gentle Nudge Towards Safety: Experimental Validation of the Potential Field Driver Assistance System

Eric J. Rossetter
Design Division
Dept. of Mechanical Engineering
Stanford University
Stanford, California 94305-4021
Email: ejross@cdr.stanford.edu

Joshua P. Switkes
Design Division
Dept. of Mechanical Engineering
Stanford University
Stanford, California 94305-4021
Email: switkesj@stanford.edu

J. Christian Gerdes
Design Division
Dept. of Mechanical Engineering
Stanford University
Stanford, California 94305-4021
Email: gerdes@cdr.stanford.edu

Abstract

This paper presents experimental validation of a driver-assistance lanekeeping system based on a potential field framework. This system is implemented on a 1997 Corvette modified for steer-by-wire capability. This testbed has no mechanical connection between the hand wheel and road wheels, allowing the lanekeeping system to add control inputs independently from the driver. The potential field framework provides an intuitive approach for combining commands from the controller and driver. The state estimation and lane position errors are obtained using the Global Positioning System (GPS) and precision road maps. Preliminary experimental data shows that this control scheme performs extremely well for driver assistance and closely matches simulation results, verifying previous theoretical guarantees for safety.

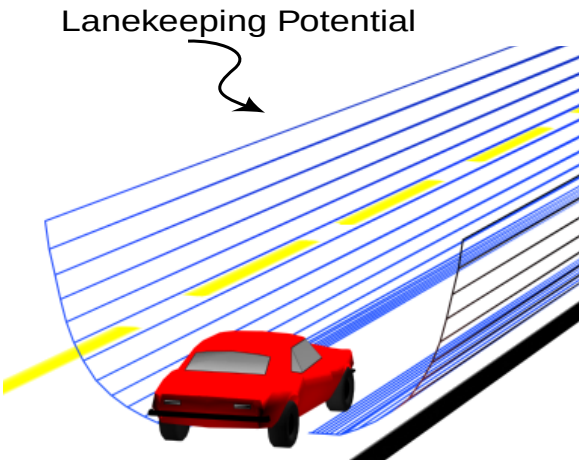

Figure 1: Potential Field for Lanekeeping

1 Introduction

With steer-by-wire on the horizon for production vehicles, it will soon be possible to incorporate active safety features such as lanekeeping assistance. These systems must provide some level of increased safety while working cooperatively with the driver. A lanekeeping assistance system designed to achieve these goals is the potential field framework proposed by Gerdes and Rossetter [4]. Under this approach, control forces are derived from artificial potential functions to control the vehicle towards safe regions of the road. The potential function is an intuitive way to represent hazard level, with a large potential corresponding to a high level of hazard. For lanekeeping, the potential function minimum is at lane center, with height increasing towards the lane edges (Figure 1). Unlike autonomous systems, this driver assistance system adds control inputs on top of the driver's commands and does not alter the underlying vehicle dynamics. Therefore, a driver will not notice the control if he or she is driving normally (i.e. close to the minimum of the potential). If, however, the vehicle deviates from lane center, the potential field controller will add steering commands, keeping the vehicle from leaving the lane.

The experimental test bed is a 1997 C5 Corvette modified to include a steer-by-wire system with no mechanical connection between the handwheel and the road wheels (Figure 2) [12]. The vehicle combines information from inertial navigation system (INS) sensors and the Global Positioning System with differential corrections (DGPS) to obtain vehicle heading and position. Differential GPS has been used as a sensing system for autonomous vehicle control by several groups. In 1992 Crow and Manning [2] demonstrated the use of DGPS for low speed autonomous vehicle control. Similar systems have been developed and tested by Farrell and Barth [3], Omae and Fujioka [5] as well as Schiller et al [10]. Another unique use of DGPS and a multi-antenna system for attitude was the autonomous control of a farm tractor by Rekow et al [6]. For these autonomous systems the vehicles used an actuator directly applying torque to the steering column. Although this type of system is fine for autonomous vehicles, the steer-by-wire setup allows steering

commands that are determined by a combination of driver and controller inputs. This setup is ideal for the implementation of the potential field driver assistance system that smoothly combines the driver and controller objectives.

Figure 2: Steer-by-Wire Corvette

The paper will discuss the potential field control algorithm, controller implementation on the steer-by-wire Corvette testbed, and preliminary experimental results. By design, the potential field framework is not a tracking controller, but the results show that the system can keep the vehicle from leaving the lane without driver inputs. Initial testing also indicates that this system works extremely well with the driver and will be unobtrusive for freeway lanekeeping. The experimental data matches quite well with simulation of a simple 2-DOF bicycle model. This predictability through simple simulation is extremely beneficial because theoretical performance guarantees, based on these relatively simple dynamics, will work well in practice.

2 Vehicle Dynamics

For this lanekeeping system, the longitudinal velocity is not controlled. As a result, only the lateral and yaw dynamics are developed in this section. The longitudinal velocity appears in these equation and need not be constant for the results that follow. The lateral vehicle dynamics are well described using the simple 2-DOF bicycle model shown in Figure 3. The equations of motion are given by

$$m\dot{U}_y = F_{yf}cos\delta + F_{yr} - mrU_x \quad (1)$$
$$I_z\dot{r} = aF_{yf}cos\delta - bF_{yr} \quad (2)$$

where

$$F_{yf} = F_{ylf} + F_{yrf} \quad (3)$$
$$F_{yr} = F_{ylr} + F_{yrr} \quad (4)$$

Assuming equal slip angles on the left and right tires and making small angle approximations

$$\alpha_f = \frac{U_y + ra}{U_x} - \delta \quad (5)$$
$$\alpha_r = \frac{U_y - rb}{U_x} \quad (6)$$
$$(7)$$

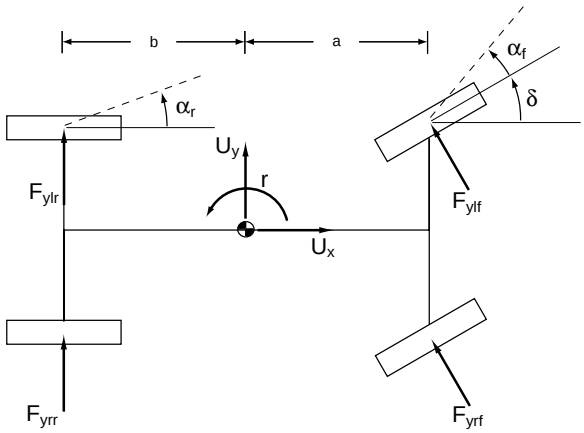

Figure 3: 2 DOF Bicycle Model

Using a linear tire model the lateral tire forces are given by

$$F_{yf} = -C_f\alpha_f \quad (8)$$
$$F_{yr} = -C_r\alpha_r \quad (9)$$

where C_f and C_r are the front and rear cornering stiffnesses, respectively. Substituting the forces into the equations of motion and making small angle approximations on the steering angle yields

$$m\dot{U}_y = -C_f\left(\frac{U_y + ra}{U_x} - \delta\right) - C_r\left(\frac{U_y - rb}{U_x}\right) - mrU_x \quad (10)$$
$$I_z\dot{r} = -aC_f\left(\frac{U_y + ra}{U_x} - \delta\right) + bC_r\left(\frac{U_y - rb}{U_x}\right) \quad (11)$$

With a steer-by-wire vehicle the components in the equations of motion can be grouped into uncontrolled drift terms and controlled terms involving the steering.

$$M\ddot{q} = f(\dot{q}) + g(\delta) \quad (12)$$

where $\dot{q} = [U_y\ r]^T$, M is the positive definite mass matrix, $f(\dot{q})$ contains the terms that are not influenced by the control vector and $g(\delta)$ has the remaining controlled terms.

$$M = \begin{bmatrix} m & 0 \\ 0 & I_z \end{bmatrix} \quad (13)$$
$$f(\dot{q}) = \begin{bmatrix} -C_r(\frac{U_y - rb}{U_x}) - C_f(\frac{U_y + ra}{U_x}) - mrU_x \\ -aC_f(\frac{U_y + ra}{U_x}) + bC_r(\frac{U_y - rb}{U_x}) \end{bmatrix} \quad (14)$$
$$g(\delta) = \begin{bmatrix} C_f\delta \\ aC_f\delta \end{bmatrix} \quad (15)$$

The overall steering angle, δ, is determined by a combination of the potential field controller and the driver commanded steering angle as described in the following section.

3 Potential Field Control

The lanekeeping system operates by comparing the position of the vehicle to a digital map of the road centerline. The

relative coordinates between the vehicle's global position and the map are defined by $w = [s\ e\ \Delta\psi]^T$ where s is the distance along the roadway, e is the distance of the vehicle's center of gravity from the lane center and $\Delta\psi$ is the heading angle error of the vehicle relative to the desired path (Figure 4).

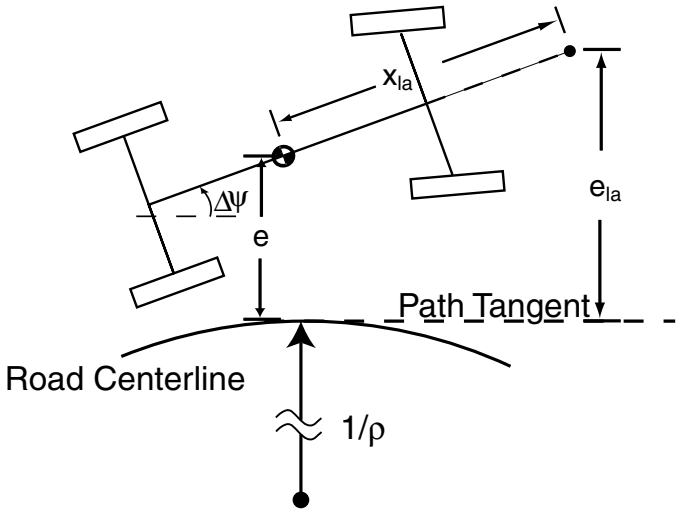

Figure 4: Global Coordinates

Transformation between the relative coordinates and body fixed velocities, $\dot{q_v} = [U_x\ U_y\ r]^T$, is achieved with

$$\frac{\partial \dot{w}}{\partial \dot{q_v}} = \frac{\partial w}{\partial q_v} = \begin{bmatrix} \cos\Delta\psi & -\sin\Delta\psi & 0 \\ \sin\Delta\psi & \cos\Delta\psi & 0 \\ 0 & 0 & 1 \end{bmatrix} \tag{16}$$

The control law introduced by Gerdes and Rossetter [4] applies a control force to the vehicle derived from the gradient of an artificial potential function. For lanekeeping, a simple quadratic potential function is used with the minimum at the lane center. Since the hazards are fixed in the environment (in this case, the lane edges) it makes sense to define the potential relative to the desired path. For high speed stability it is necessary to incorporate a projection (lookahead) into the potential function [7]. As a result, the quadratic potential used to generate the desired control force is a function of this projected offset from the lane center, e_{la}.

$$V(e_{la}) = k(e_{la})^2 = k(e + x_{la}\sin\Delta\psi)^2 \tag{17}$$

where x_{la} is the projected distance in front of the vehicle and k is the potential field gain.

Since only the steering can be controlled in the vehicle, the control force derived from the potential function will effect both the lateral and yaw motions of the vehicle. Using the potential function described in Equation 17 the control law is given by

$$g(\delta) = g(\delta_{driver}) + \begin{bmatrix} -\frac{\partial V}{\partial e}cos\Delta\psi \\ -a\frac{\partial V}{\partial e}cos\Delta\psi \end{bmatrix} \tag{18}$$

The equations of motion in the previous section can now be written as

$$M\ddot{q} = f(\dot{q}) + g(\delta_{driver}) + \begin{bmatrix} -\frac{\partial V}{\partial e}cos\Delta\psi \\ -a\frac{\partial V}{\partial e}cos\Delta\psi \end{bmatrix} \tag{19}$$

In essence, this low level control law simply adds conservative forces to the existing vehicle dynamics. This approach has several benefits. The idea of using control to add 'artificial' potential energy to the system can be extended to find a Lyapunov function for the lateral and yaw dynamics of the vehicle [8]. This function defines a realistic reachable set for these dynamics and can be used to scale the potential function in order to guarantee that lane boundaries will not be crossed.

4 Control Structure

Controlling the vehicle relative to lane center requires an accurate estimation of vehicle position and heading deviation (Figure 4). The control structure used is shown in Figure 5. Carrier phase DGPS provides absolute position information with an accuracy of 1cm CEP (σ =0.2cm), while a Novatel Beeline two-antenna GPS system determines the vehicle heading to within .4°. The GPS measurements are accurate but have a slow update rate (10Hz for DGPS and 5Hz for heading). To have an accurate estimate of state between GPS updates, accelerations and yaw rate from an Inertial Measurement Unit are integrated using two Kalman filters described in Section 6. The Kalman filters output the vehicle's position and heading. By comparing these values to a precision map of the road, the error in lateral position and heading is determined. This error is used by the potential field controller to calculate the steering addition needed [12].

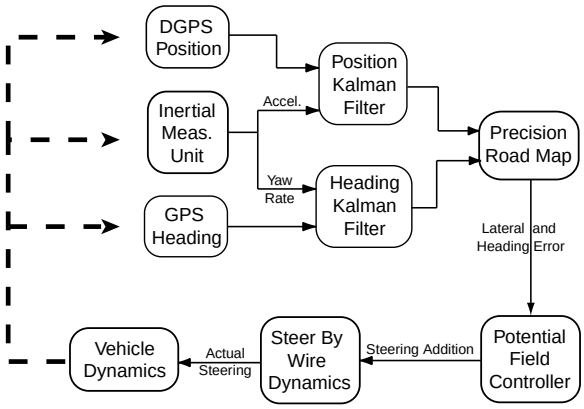

Figure 5: Control Structure for Vehicle Lane-Keeping

5 Precision Maps

The map making process consists of driving the road loop at constant speed and recording position measurements from

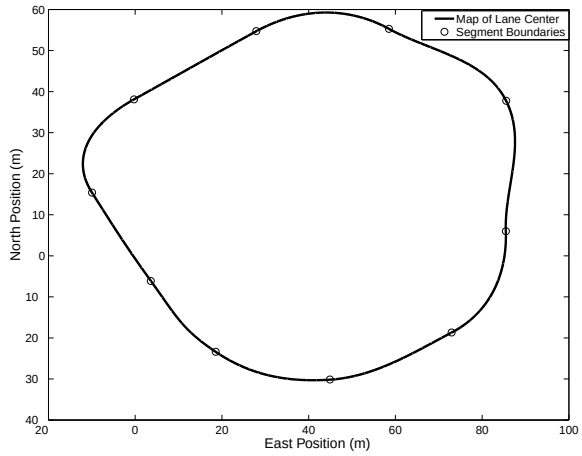

Figure 6: Map of Lane Center Showing Segment Boundaries

DGPS. A smooth map is generated from this data using constrained least squares. This map consists of a predetermined number of segments, each of which is a parametric polynomial function of the parameter σ [11](Figure 6). The number of segments is chosen so that each segment will capture a feature of the road while the constant speed ensures that the density of data points is roughly uniform. For simplicity the segments contain equal numbers of data points. The polynomials describing each segment are given by

$$Y_i(\sigma) = a_{yi}\sigma^3 + b_{yi}\sigma^2 + c_{yi}\sigma + d_{yi} \quad (20)$$

$$X_i(\sigma) = a_{xi}\sigma^3 + b_{xi}\sigma^2 + c_{xi}\sigma + d_{xi} \quad (21)$$

where a_{yi} and a_{xi} denote the ith coefficient in the polynomial for Y and X, and σ varies from 0 to 1 on each segment.

The determination of the polynomial coefficients is formed as a constrained least squares problem [1]. To setup this problem, the unconstrained least squares solution is needed.

$$x_{in} = Hk_{xls} \quad (22)$$

$$y_{in} = Hk_{yls} \quad (23)$$

where k_{xls} and k_{yls} contain the best fit polynomial coefficients for all the segments.

$$k_{xls} = \begin{pmatrix} a_{x1} & b_{x1} & c_{x1} & d_{x1} & \dots & a_{xn} & b_{xn} & c_{xn} & d_{xn} \end{pmatrix}^T \quad (24)$$

$$k_{yls} = \begin{pmatrix} a_{y1} & b_{y1} & c_{y1} & d_{y1} & \dots & a_{yn} & b_{yn} & c_{yn} & d_{yn} \end{pmatrix}^T \quad (25)$$

$$H = \begin{pmatrix} \bar{\sigma}^3 & \bar{\sigma}^2 & \bar{\sigma} & 1 & 0 & 0 & 0 & 0\dots \\ 0 & 0 & 0 & 0 & \bar{\sigma}^3 & \bar{\sigma}^2 & \bar{\sigma} & 1\dots \\ \vdots & \vdots & \vdots & \vdots & \vdots & \vdots & \vdots & \ddots \end{pmatrix} \quad (26)$$

where $\bar{\sigma}$ denotes the entire σ vector, ranging from 0 to 1, of length equal to the number of data points in the segment. The unconstrained solution is then found as the least squares solution of the above, or

$$k_{yls} = (H^T H)^{-1} H^T y_{in} \quad (27)$$

$$k_{xls} = (H^T H)^{-1} H^T x_{in} \quad (28)$$

The standard least squares solution does not ensure that the map will be continuous or smooth at the segment boundaries.

For a useful map, we must require that it be continuous at segment ends, and that the slope be continuous at segment boundaries.

$$Y_i(1) = Y_{i+1}(0) \quad (29)$$

$$X_i(1) = X_{i+1}(0) \quad (30)$$

$$\frac{\partial Y_i}{\partial \sigma}(1) = \frac{\partial Y_{i+1}}{\partial \sigma}(0) \quad (31)$$

$$\frac{\partial X_i}{\partial \sigma}(1) = \frac{\partial X_{i+1}}{\partial \sigma}(0) \quad (32)$$

(33)

Thus, we must require that

$$a_{yi} + b_{yi} + c_{yi} + d_{yi} = d_{yi+1} \quad (34)$$

$$a_{xi} + b_{xi} + c_{xi} + d_{xi} = d_{xi+1} \quad (35)$$

$$3a_{yi} + 2b_{yi} + c_{yi} = c_{yi+1} \quad (36)$$

$$3a_{xi} + 2b_{xi} + c_{xi} = c_{xi+1} \quad (37)$$

Using these constraint equations, the problem can be reformulated as a constrained least squares problem in which these equality constraints are placed on the problem in the form of a matrix equation. This matrix equation is not a minimization, but rather a series of equations that must be satisfied:

$$Ak_{xopt} = 0 \quad (38)$$

$$Ak_{yopt} = 0 \quad (39)$$

where the A matrix is formed to constrain the continuity and smoothness at segment boundaries.

In order to form a closed map, the last rows of the A matrix must enforce the continuity and smoothness between the final and first segments of the map, in the same way outlined above.

With the problem formulated in this way, we can find the constrained least squares solution as

$$k_{yopt} = k_{yls} - (H^T H)^{-1} A^T [A(H^T H)^{-1} A^T]^{-1} Ak_{yls} \quad (40)$$

$$k_{xopt} = k_{xls} - (H^T H)^{-1} A^T [A(H^T H)^{-1} A^T]^{-1} Ak_{xls} \quad (41)$$

6 Kalman Filters

As shown in Figure 5, the control structure uses two Kalman filters that integrate INS sensors with GPS information for high update heading and position values. For the heading Kalman filter, a linear dynamic system can be constructed using the yaw rate as an input and the heading from a two-antenna GPS system for the measurement update [9].

$$\begin{bmatrix} \dot{\psi} \\ \dot{r}_{bias} \end{bmatrix} = \begin{bmatrix} 0 & -1 \\ 0 & 0 \end{bmatrix} \begin{bmatrix} \psi \\ r_{bias} \end{bmatrix} + \begin{bmatrix} 1 \\ 0 \end{bmatrix} r_m + \text{noise} \quad (42)$$

$$\psi_m{}^{GPS} = \begin{bmatrix} 1 & 0 \end{bmatrix} \begin{bmatrix} \psi \\ r_{bias} \end{bmatrix} + \text{noise} \quad (43)$$

where ψ is the heading, r_m is the measured yaw rate, r_{bias} is the yaw rate sensor bias, and ${\psi_m}^{GPS}$ is the GPS heading from the two-antenna GPS system.

The second Kalman filter uses lateral and longitudinal accelerations along with DGPS position information to obtain a high update global position of the vehicle. For this Kalman filter the linear dynamic system uses the vehicle's lateral and longitudinal accelerations as inputs and the DGPS east and north positions for the measurement update. The heading output of the first filter is used to transform the accelerations from body fixed to global coordinates.

$$\begin{bmatrix} \dot{P}_N \\ \ddot{P}_N \\ \dot{a}_{x_{bias}} \\ \dot{P}_E \\ \ddot{P}_E \\ \dot{a}_{y_{bias}} \end{bmatrix} = A \begin{bmatrix} P_N \\ \dot{P}_N \\ a_{x_{bias}} \\ P_E \\ \dot{P}_E \\ a_{y_{bias}} \end{bmatrix} + B \begin{bmatrix} a_{xm} \\ a_{ym} \end{bmatrix} + \text{noise} \qquad (44)$$

where P_N and P_E are the north and east position of the vehicle, respectively, a_{xbias} is the longitudinal accelerometer bias, $a_{y_{bias}}$ is the lateral accelerometer bias, a_{xm} is the measured longitudinal acceleration, and a_{ym} is the measured lateral acceleration. The matrices A and B are

$$A = \begin{bmatrix} 0 & 1 & 0 & 0 & 0 & 0 \\ 0 & 0 & -cos\psi & 0 & 0 & sin\psi \\ 0 & 0 & 0 & 0 & 0 & 0 \\ 0 & 0 & 0 & 0 & 1 & 0 \\ 0 & 0 & sin\psi & 0 & 0 & cos\psi \\ 0 & 0 & 0 & 0 & 0 & 0 \end{bmatrix} \qquad (45)$$

$$B = \begin{bmatrix} 0 & 0 \\ cos\psi & -sin\psi \\ 0 & 0 \\ 0 & 0 \\ -sin\psi & -cos\psi \\ 0 & 0 \end{bmatrix} \qquad (46)$$

with the heading, ψ, coming from the heading Kalman filter. The measurement update equation is

$$\begin{bmatrix} P_N^{GPS} \\ P_E^{GPS} \end{bmatrix} = \begin{bmatrix} 1 & 0 & 0 & 0 & 0 & 0 \\ 0 & 0 & 0 & 1 & 0 & 0 \end{bmatrix} \begin{bmatrix} P_N \\ \dot{P}_N \\ a_{xbias} \\ P_E \\ \dot{P}_E \\ a_{y_{bias}} \end{bmatrix} + \text{noise} \qquad (47)$$

where P_N^{GPS} and P_E^{GPS} are the north and east position measurements from DGPS.

The heading and position outputs from these filters are used to calculate the lateral and heading error of the vehicle relative to the stored map. These errors are used by the potential field controller to add steering inputs, moving the vehicle towards the desired path.

	7m/s Run	11m/s Run
P.F. gain k	4350	10000
x_{la} (m)	5.0	10.5
m (kg)	1600	1600
I_z (N/m^2)	2500	2500
C_f (N/rad)	110000	110000
C_r (N/rad)	100000	100000
a (m)	1.3	1.3
b (m)	1.3	1.3

Table 1: Controller and Vehicle Parameters

7 Results and Simulation

Figure 7 shows an excellent match between experimental results and simulation using the simple bicycle model (Table 1), for a test run at about 7m/s. This data was collected with no driver steering input, and consists of two laps around the test map. The two laps are indistinguishable on this scale, showing extremely good repeatability for the system. Figure 8 and 9 show the map and lateral error for a test run at 11m/s. These higher speed runs were conducted on the West Ramp and West Parallel of Moffett Federal Airfield. The lateral error in simulation versus experiment differ by no more than 5cm. The close match to simulation is quite remarkable considering the simple model used as well as the absence of noise and steering dynamics in the simulation. The simulation does not take into account the surface of the testing area, which contained numerous pavement seams and rectangular holes containing tie-downs for aircraft. These results verify that the vehicle remains in the lane without driver steering commands. The repeatability of the vehicle motion is significant because it creates a response that is easily predicted by the driver. There are no unexpected motions that might force the driver to make unnatural steering commands to remain on the path (i.e. the driver steering the wrong direction around a corner).

The simple simulation's close match to the experimental results allows for offline design and scaling of the potential function. The predictability of the system response using a simple vehicle model also ensures that theoretical reachability results for the lateral motion of the vehicle are applicable to the physical system. This theoretical result is a powerful tool, yielding potential field gains that guarantee the lane-keeping ability of the system.

8 Conclusion

This paper presented initial experimental results for the potential field assistance system. The system performed extremely well and almost exactly as predicted by simulation. The success of these experiments confirms that the system can be used to avoid lane excursions in the absence of driver inputs and can be designed using theoretical performance guarantees. The test setup also verifies the feasi-

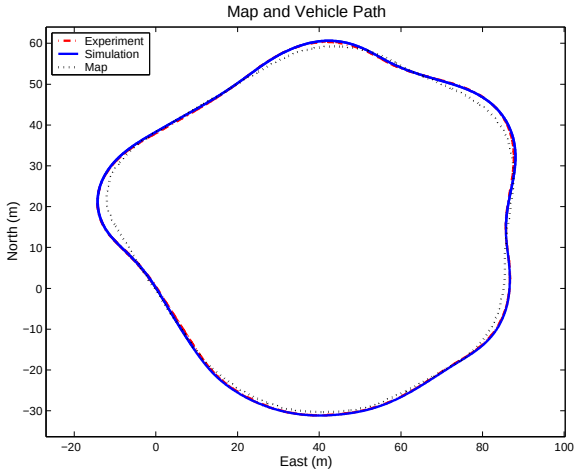

Figure 7: Vehicle Path Relative to Map

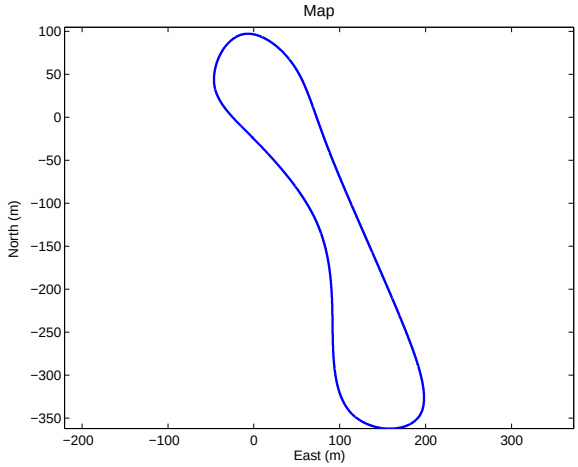

Figure 8: Moffett Field Map

bility of using GPS data and INS sensors to detect lane position for smooth and comfortable lanekeeping assistance. Future work will focus on driver feel including handwheel force feedback and experimental verification of lanekeeping guarantees.

Acknowledgements

The authors would like to thank Michael Grimaldi, Robert Wiltse and Pamela Kneeland at General Motors Corporation for the donation of the Corvette and the GM Foundation for the grant enabling its conversion to steer-by-wire. The authors would also like to thank Dr. Skip Fletcher, T.J. Forsyth, Geary Tiffany and Dave Brown at the NASA Ames Research Center for the use of Moffett Federal Airfield. This material is based upon work supported by the National Science Foundation under Grant No. CMS-0134637 with additional support from a National Science Foundation Graduate Research Fellowship.

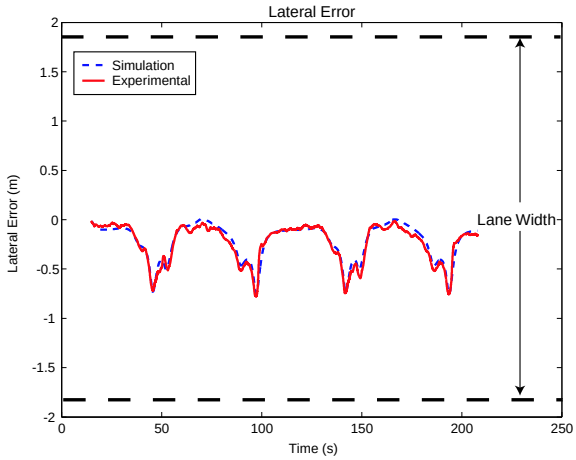

Figure 9: Lateral Error: Experiment vs. Simulation

References

[1] Ake Bjorck. *Numerical Methods for Least Squares Problems*. SIAM, Philadelphia, PA, 1996.

[2] S.C. Crow and F.L. Manning. Differential GPS Control of Starcar 2. *Journal of the Institute of Navigation*, 39:383–405, Winter 1992.

[3] J. Farrell and M. Barth. Integration of GPS-aided INS into AVCSS. Technical Report MOU 374, California PATH Program, 2000.

[4] J.C. Gerdes and E.J. Rossetter. A Unified Approach to Driver Assistance Systems Based on Artificial Potential Fields. ASME *Journal of Dynamic Systems, Measurement, and Control*, 123:431–438, September 2001.

[5] M. Omae and T. Fujioka. DGPS-Based Position Measurement and Steering Control for Automatic Driving. In *Proceedings of the American Control Conference*, 1999.

[6] A. Rekow, T. Bell, D. Bevly, and B. Parkinson. System Identification and Adaptive Steering of Tractors Utilizing Differential Global Positioning System. *Journal of Guidance, Control, and Dynamics*, 22:671–674, Sept.-Oct. 1999.

[7] E.J. Rossetter and J.C. Gerdes. A Study of Lateral Vehicle Control Under a 'Virtual' Force Framework. In *Proceedings of the International Symposium on Advanced Vehicle Control (AVEC)*, 2002.

[8] E.J. Rossetter and J.C. Gerdes. Performance Guarantees for Hazard Based Lateral Vehicle Control. In *Proceedings of the ASME International Mechanical Engineering Congress and Exposition*, 2002.

[9] J. Ryu, E.J. Rossetter, and J.C. Gerdes. Vehicle Sideslip and Roll Parameter Estimation Using GPS. In *Proceedings of the International Symposium on Advanced Vehicle Control (AVEC)*, 2002.

[10] B. Schiller, V. Morellas, and M. Donath. Collision avoidance for highway vehicles using the virtual bumper controller. In *Proceedings of the IEEE International Symposium on Intelligent Vehicles*, 1998.

[11] S. Schrödl, S. Rogers, and C. Wilson. Map Refinement from GPS Traces. Technical Report 6, Daimler Chrysler RTC North America, 2000.

[12] P. Yih, J. Ryu, and J.C. Gerdes. Modification of Vehicle Handling Characteristics via Steer-By-Wire. In *Proceedings of the American Control Conference*, 2003.